THE JOURNAL OF PHYSICAL CHEMISTRY C

ARTICLE

pubs.acs.org/JPCC

Homogeneous Nucleation of Graphitic Nanostructures from Carbon Chains on Ni(111)

Daojian Cheng,[†,‡] Giovanni Barcaro,[§] Jean-Christophe Charlier,[∥] Marc Hou,[‡] and Alessandro Fortunelli*[,§]

[†]State Key Laboratory of Organic−Inorganic Composites, College of Chemical Engineering, Beijing University of Chemical Technology, Beijing 100029, People's Republic of China

[‡]Physique des Solides Irradiés et des Nanostructures CP234, Faculté des Sciences, Université Libre de Bruxelles, Boulevard du Triomphe, B-1050 Bruxelles, Belgium

[§]CNR-IPCF, Istituto per i Processi Chimico-Fisici, Molecular Modeling Laboratory, via G. Moruzzi 1, I-56124, Pisa, Italy

[∥]Institute of Condensed Matter and Nanosciences (IMCN), Université catholique de Louvain, Place Croix du Sud 1 (NAPS-Boltzmann), B-1348 Louvain-la-Neuve, Belgium

Supporting Information

ABSTRACT: The structure, energetics, and mobility of carbon aggregates up to 10 atoms on the Ni(111) surface are investigated via first-principles simulations. Chain configurations are predicted to be thermodynamically favored over rings and present a high mobility (with long chains diffusing even faster than adatoms), whereas branched configurations are much less mobile but kinetically robust, as they present substantial energy barriers for interconversion into other species. A model of growth via homogeneous nucleation is proposed in which incoming C atoms generate chains which diffuse rapidly and collect less mobile adatoms in their channels until they meet in an unfavorable configuration and start networking giving rise to starlike branching points, which are homologous to graphene and act as the nuclei of growth. It is argued that the proposed homogeneous nucleation mechanism should be observed experimentally, especially in mild conditions and on low-defect Ni(111) surfaces.

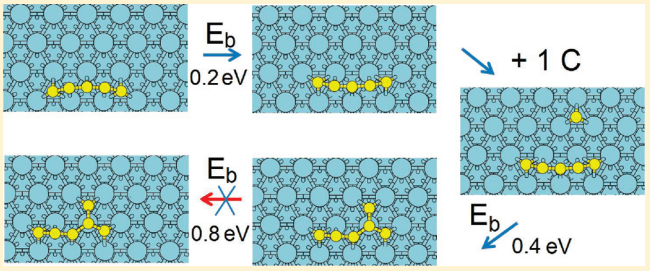

INTRODUCTION

Ni particles are known to be excellent catalysts for the growth of carbon-based nanomaterials such as tubes and fibers[1] which are expected to play a crucial role in future electronics.[2] Despite considerable efforts, however, the mechanisms of the involved catalytic processes still present unresolved issues, especially at low temperature which is currently targeted as more economical and to enable use of more sensitive substrates and/or to better control the growth kinetics.[3] Previous studies have mainly dealt with the early stages of growth, focusing in particular on the nucleation step[4] in which a stable carbon aggregate is formed which then grows by addition of smaller species. In this context, a model of heterogeneous nucleation is usually assumed in which graphitic structures such as graphene sheets develop at step edges or other strong trapping centers,[5,6] i.e., extended defects on the surface of the metal particles, either native or induced by the presence of the carbon species itself.[7] In this model, the role played by the good epitaxial match between graphene and the Ni(111) surface, one of the reasons to use Ni particles as catalysts, is usually overlooked, with few very recent exceptions.[8] One characteristics of Ni in fact is that its first-neighbor distance in the bulk (2.49 Å) is almost identical to the in-plane lattice parameter of graphite (2.46 Å), with a lattice mismatch slightly larger than 1%. Hence, the growth of graphitic planar structures is expected to be the easiest on Ni(111) surfaces. In the present paper, based on first-principles (density-functional theory, DFT) simulations, we propose an alternative mechanism of homogeneous nucleation in which formation, diffusion, and growth of small carbon clusters occur on the undefected Ni(111) surface. Knowledge on the structure and energetics of adsorption and the mobility of such species will allow us to contrive a picture of the early stages of growth of carbon nanostructures on this system. We argue that the proposed homogeneous nucleation mechanism should be observed experimentally, in particular at low temperature and possibly in competition with the usually assumed heterogeneous nucleation one. The article is organized as follows. After a brief section in which we validate our computational approach by comparison with previous work, results are presented and discussed in the central section. The main conclusions are then summarized. A methodological section concludes the article.

Received: March 25, 2011
Revised: April 27, 2011
Published: May 12, 2011

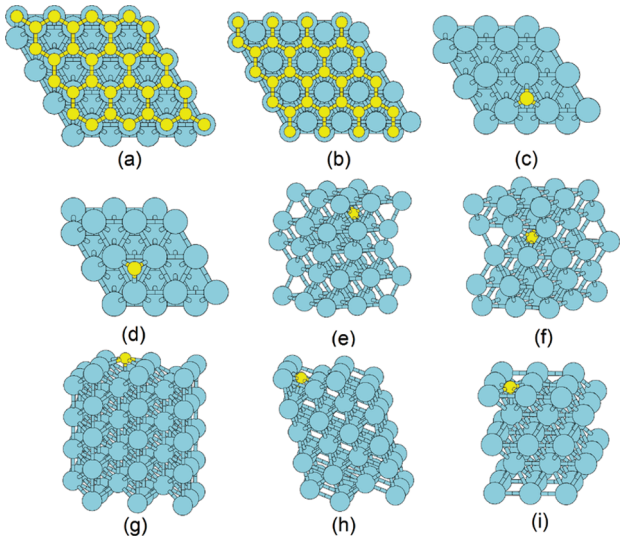

Figure 1. Pictorial views of the carbon adsorption on Ni surfaces: (a) top-fcc graphene on Ni(111); (b) hcp-fcc graphene on Ni(111); (c, d) adatom fcc (c) and hcp (d) sites on Ni(111); (e) subsurface atom on Ni(111); (f) single atom in bulk Ni; (g) 5-fold site on Ni(110); (h) 5-fold site on Ni(113); (i) 5-fold site on Ni(100). Carbon atoms are in yellow, nickel atoms in blue.

COMPARISON WITH PREVIOUS WORK

The adsorption mechanisms of a single C atom or a graphene monolayer on various Ni surfaces have been investigated in previous studies[5,9−12] and are used as validation tests of our computational approach. Defining the adsorption energy E_{ads} as the energy difference between the local minimum configuration of the composite carbon-cluster + metal-surface system and the relaxed metal surface plus carbon atoms in the gas phase, our DFT calculations predict the following energy ordering for the E_{ads} values (given in parentheses in electronvolts)

$$\{111\}_{fcc}(-6.63) > \{111\}_{hcp}(-6.68) > \text{bulk}(-7.0) > \{111\}_{subsurf}(-7.25) > \{110\}_{5\text{-fold}}(-7.25)\ \text{eV} > \{113\}_{5\text{-fold}}(-7.64) > \text{graphene}\{111\}_{top\text{-}fcc}(-7.85) > \{100\}(-7.88)$$

where $\{hkl\}$ represents a Ni(hkl) surface, the "fcc", "hcp", and "subsurf" subscripts refer to the corresponding adsorption sites on the Ni(111) surface, the "5-fold" subscript refers to the most stable adsorption site on the Ni(113) surface, "bulk" refers to adsorption in bulk fcc Ni, and "graphene" stands for the adsorption energy per carbon atom of a graphene monolayer on top-fcc sites of Ni(111)—see Figure 1 for a pictorial view of adsorption sites.

In agreement with previous studies[5,9−12] and physical considerations on bond-strength/coordination-number relationships, we find that C binding is stronger to low-coordinated Ni atoms and that on a perfect Ni(111) surface a single C atom preferentially adsorbs on a subsurface site, while dissolution into the bulk is the next favorable position and the adatom is the least stable one. The subsurface configuration is more stable with respect to epitaxial adsorption or dissolution into the bulk because it strikes the balance between the maximization of the C coordination and the minimization of the energy stored in elastic stress of the Ni lattice. It can be noted that octahedral subsurface and bulk absorption site are considered here, as the other possible tetrahedral sites are too small to accommodate a carbon atom.[13] A C adatom on Ni(111) can jump to a subsurface site: crossing of the {111} surface is experimentally observed to occur spontaneously at temperatures above 770 K[14] and indeed we calculate the energy barrier for the jump from adatom to subsurface to be 0.6 eV, while the reverse path (corresponding to the release of subsurface C to the surface) has a barrier of 1.2 eV (in agreement with previous calculations[13]). Similarly, the energy barrier to release a C atom from a 5-fold site of the (113) surface, which is a good model for a line step defect on the (111) surface, is 1.2 eV. Subsurface or step sites can thus act as storage sites for carbon on the Ni(111) surface in the initial stages of growth, but at the price of significant energy barriers for C release. Moreover the fact that E_{ads} has its second largest value in graphene confirms

Table 1. Energies and Geometries of Selected Small Carbon Clusters on Various Ni Surfaces[a]

system	z_{min}/z_{max}	E_{ads}	E_{bnd}	E_{adh}	σ
graphene $\{111\}_{top\text{-}fcc}$	2.12	−7.84	−7.84	−0.00	<0.01
graphene $\{111\}_{hcp\text{-}fcc}$	4.73	−7.85	−7.84	−0.01	<0.01
$C_1\{111\}_{hcp}$	0.97	−6.68		−6.78	0.10
$C_1\{111\}_{fcc}$	1.03	−6.63		−6.73	0.10
$C_1\{111\}_{subsurf}$	−0.91	−7.25		−7.64	0.39
$C_1\{100\}_{5\text{-fold}}$	0.27	−7.88		−8.06	0.18
$C_1\{110\}_{5\text{-fold}}$	0.19	−7.25		−7.44	0.19
$C_1\{110\}_{long\text{-}bridge}$	0.45	−6.97		−7.59	0.62
$C_1\{113\}_{5\text{-fold}}$	−0.22	−7.64		−7.85	0.21
$C_2\ \{111\}_{hcp\text{-}fcc}$	1.25	−6.88	−3.49	−3.51	0.12
$C_2\{111\}_{subsurf}$	−0.28/−0.92	−6.30	−3.33	−3.98	1.01
$C_2\{111\}_{vertical}$	−0.73/0.74	−5.77	−3.11	−3.45	0.79
$C_3\{111\}_{fcc\text{-}hcp\text{-}fcc}$	1.25/1.66	−6.93	−4.9	−2.1	0.07
$C_3\{111\}_{hcp\text{-}fcc\text{-}hcp}$	1.24/1.63	−6.90	−4.9	−2.07	0.07
$C_{4,L}\{111\}$	1.30/1.65	−6.98	−5.18	−1.85	0.05
$C_{4,S}\{111\}_{fcc\text{-}fcc\text{-}fcc\text{-}top}$	1.18/1.65	−6.80	−4.16	−2.75	0.10
$C_{4,S}\{111\}_{hcp\text{-}hcp\text{-}hcp\text{-}fcc}$	1.21/1.63	−6.69	−4.16	−2.63	0.09
$C_{4,S}\{111\}_{top\text{-}top\text{-}top\text{-}hcp}$	1.78/2.05	−5.78	−4.17	−1.63	0.02
$C_{4,S}\{111\}_{top\text{-}top\text{-}top\text{-}top}$	1.33/1.82	−5.91	−4.86	−1.13	0.07
$C_{5,L}\{111\}$	1.30/1.74	−6.98	−5.62	−1.42	0.06
$C_{5,R}\{111\}$	1.33/1.42	−6.64	−4.86	−1.92	0.14
$C_{6,L}\{111\}$	1.30/1.87	−7.00	−5.74	−1.32	0.05
$C_{6,S}\{111\}$	1.24/1.80	−6,89	−4.94	−2.03	0.08
$C_{6,R}\{111\}$	1.40/1.41	−6.78	−5.45	−1.46	0.13
$C_{6,DS}\{111\}$	1.05/1.54	−6.77	−4.51	−2.36	0.10
$C_{7,L}\{111\}$	1.30/2.02	−7.00	−5.92	−1.12	0.05
$C_{7,R}\{111\}$	1.19/1.70	−6.81	−5.35	−1.58	0.11
$C_{8,L}\{111\}$	1.32/1.98	−7.00	−5.99	−1.07	0.04
$C_{8,R}\{111\}$	1.36/2.33	−6.72	−5.77	−1.03	0.09
$C_{9,L}\{111\}$	1.30/1.88	−7.00	−6.13	−0.92	0.03
$C_{9,R}\{111\}$	1.38/2.10	−6.73	−6.01	−0.78	0.06
$C_{10,L}\{111\}$	1.27/1.97	−7.00	−6.15	−0.89	0.03
$C_{10,R}\{111\}$	1.51/2.02	−6.95	−6.15	−0.84	0.04
$C_{10,DR}\{111\}$	1.36/1.83	−6.90	−5.85	−1.14	0.09

[a] E_{ads}, E_{adh}, E_{bnd}, and σ are defined in the text. z is the coordinate perpendicular to the surface (z_{min}/z_{max} refer to its minimum and maximum value), with z = 0 the Ni surface place (positive is outside). E_{ads}, E_{adh}, and σ are given per carbon atom. Energies are in electronvolts, distances in angstroms. van der Waals corrections are not included.

that, asymptotically, once the full carbon coordination is developed, the energetic preference turns into its favor. In other words adsorbed graphene will be more stable than—and incomplete graphitic-like structures will adsorb and include into their framework—other carbon species.

It can be added that van der Waals or dispersion corrections, evaluated according to a semiempirical approach,[15] are found to be essential to accurately describe the weak adhesion of graphene—or three-coordinated carbon atoms—on Ni(111). Indeed, the relative energy ordering of the top-fcc and hcp-fcc configurations (see Figure 1) are reversed by the inclusion of this contribution: without dispersion terms, the adsorption energies per carbon atom of hcp-fcc and top-fcc graphene are −7.85 and −7.84 eV, respectively; including dispersion, they are −7.93 and −8.07 eV, respectively (the difference is due to the larger adhesion of top-fcc graphene, −0.18 eV, with respect to that of hcp-fcc graphene, −0.04 eV). The top-fcc structure thus turns out to be the most stable one in agreement with experiment[16] and previous calculations[10,17] only when dispersion corrections are included. On the opposite, dispersion terms are found to make a minor difference when the carbon coordination is lower than 3 and the carbon−metal interactions are stronger, as in the case of small C aggregates. For comparison, the same E_{ads} values reported above for a single C atom or graphene on Ni surfaces including dispersion interactions are

$$\{111\}_{fcc}(-6.90) > \{111\}_{hcp}(-6.94) > \text{bulk}(-7.2) > \{110\}_{5\text{-fold}}(-7.50)\ \text{eV} > \{111\}_{subsurf}(-7.54) > \{113\}_{5\text{-fold}}(-7.84) > \text{graphene}\{111\}_{top\text{-}fcc}(-8.07) > \{100\}(-8.13)$$

where one can see that the energy ordering is basically unaltered by dispersive interactions. Dispersion terms are thus not included in Table 1 and—unless explicitly stated—in the energy values reported hereafter.

RESULTS AND DISCUSSION

The structure and energetics of small carbon clusters (C_n, $n = 1-10$) on various Ni surfaces are reported in Table 1, together with the corresponding quantities for a graphene monolayer on Ni(111). The adsorption energy E_{ads} is defined in the previous section. E_{adh} is the adhesion energy, i.e., the energy difference between the local minimum configuration of the composite carbon-cluster + metal-surface system and the metal surface plus the carbon cluster in the gas phase, both frozen in their interacting configuration. E_{bnd} is the binding energy of the carbon cluster in the gas phase in its interacting configuration. σ is the Ni stress energy, i.e., the elastic energy stored into the Ni surface due to C-induced lattice deformation. One thus has: $E_{ads} = E_{bnd} + E_{adh} + \sigma$. E_{ads}, E_{adh}, and σ are given per carbon atom.

From the results of the previous section, on a Ni(111) surface a single C atom preferentially adsorbs in a subsurface site. An inspection of Table 1 shows that by increasing the size of the C aggregate the situation changes drastically. The favorable epitaxial match of carbon aggregates on Ni(111) in fact does not transfer to subsurface (and—a fortiori—to the bulk), basically because of the strain in the Ni lattice associated with accommodating many-atom carbon species, e.g., sandwiched between (111) planes. The case of a carbon dimer is already apt to illustrate this phenomenon: a C_2 addimer ($E_{ads} = -13.75$ eV) is appreciably more stable than a subsurface dimer ($E_{ads} = -12.60$ eV),

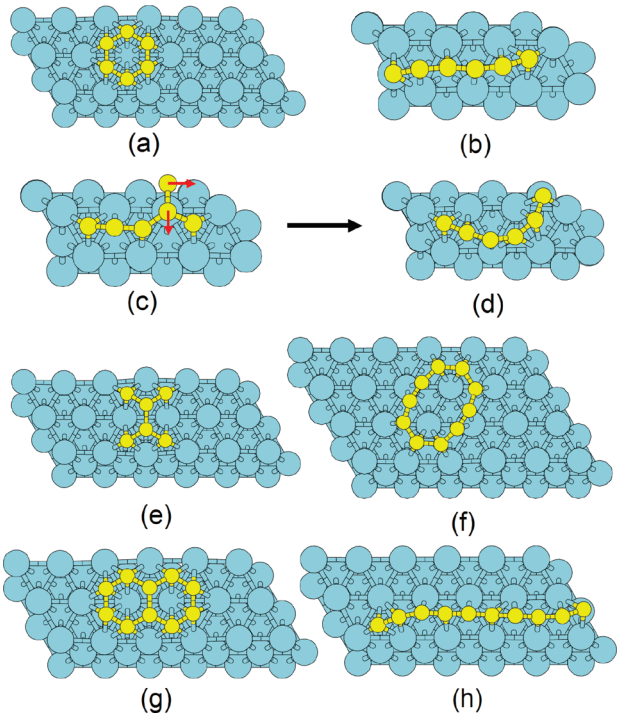

Figure 2. Optimized geometries of carbon clusters on Ni(111): (a) six-atom ring ($C_{6,R}$); (b) six-atom chain ($C_{6,L}$); (c) six-atom star ($C_{6,S}$) and its transformation mechanism into a curved linear chain (d); (e) six-atom double star ($C_{6,DS}$); (f) ten-atom ring ($C_{10,R}$); (g) ten-atom double ring ($C_{10,DR}$); (h) ten-atom chain ($C_{10,L}$). Color coding as in Figure 1.

at variance with previous predictions based on empirical approaches,[6] and most of this difference is due to the strain in the Ni structure. In this connection it should be noted that the limited size of our simulation cell entails an overestimation of the strain component for subsurface with respect to epitaxial adsorption. We estimated the relaxation of elastic stress due to the cell size by calculating the difference in elastic energy between (3×3) and a large (9×9) unit cell via classical force fields (see the Methods section for more details), and found it to be 0.5 eV, thus insufficient to revert the order of stability between epitaxial and subsurface species of a C_2 dimer. Another possible configuration for a dimer is one with a subsurface atom bound to an adatom (a "vertical" dimer: $C_2(111)_{vertical}$ in Table 1) but we found that it is even higher in energy (by more than 2.2 eV) with respect to the addimer. This excludes that subsurface atoms can act as nucleation sites for adspecies, as previously conjectured. To summarize, given the larger adsorption energies in subsurface and 5-fold sites, these represent favorite niches for storage of single carbon atoms (despite the significant escape energy barriers). However, considering additionally that first-neighbor C pairs at subsurface and at 5-fold sites repel each other by 1.0 and 0.4 eV, respectively, in the absence of reconstruction (which could be driven by this repulsion[18]), one is drawn to the conclusion that C aggregation is only favored at epitaxial sites, where the interaction between neighboring C atoms is always attractive (not only for dimers but also for larger species: the adsorption energy per carbon atom is a monotonously increasing function of the cluster size, see Table 1). One can thus expect that, possibly after some incubation time[6,19] in which storage sites are saturated, the incoming excess species or those liberated from the storage sites by random

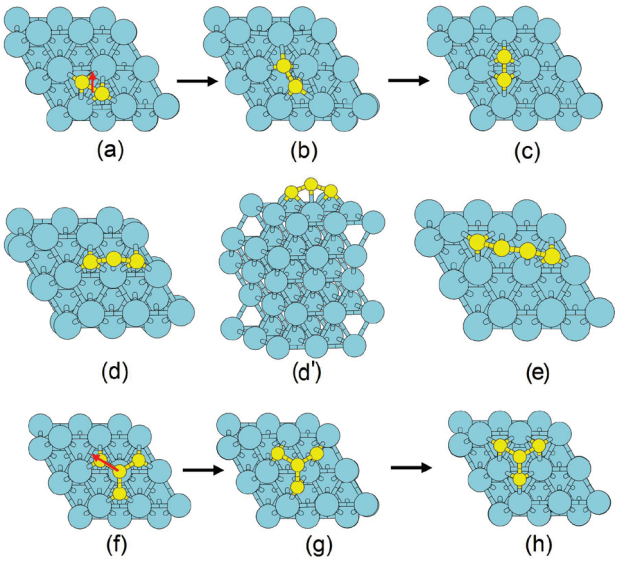

Figure 3. Pictorial views of the adsorption sites and diffusion mechanisms of selected carbon clusters on Ni(111): (a, c) hcp−fcc adsorption of a dimer and (a−c) its diffusion mechanism with (b) the saddle-point configuration; (d) top view and (d′) side view of a trimer; (e) adsorption of a chain tetramer; (f, h) adsorption of a star tetramer; (f−h) its diffusion mechanism with (g) the saddle-point configuration. Color coding as in Figure 1.

fluctuations will start diffusing and aggregating on the Ni(111) surface. These results are in agreement with previous reasoning underlining the importance of limited C solubility into Ni particles[20−22] and the current models of nascent nanotube docking onto Ni particles,[9,22] in which the key processes of growth occur *outside* the particles. A particularly interesting situation arises when the Ni(111) surface is one monolayer thick and with very few defects,[8] in which case it has been shown that large-area single crystal monolayer graphene can indeed be obtained, of great interest in applications (we became aware of this publication after the present work had already been completed). The present results perfectly apply to such an interesting case, as surface adsorption and diffusion are dominated by the Ni atoms in the topmost layer, with the further simplification that subsurface sites should be disfavored in the conditions of ref 8 and growth should only involve adspecies on a monolayer Ni(111), in agreement with our argument.

For carbon aggregates larger than a dimer, only adspecies were then studied, focusing first on the evolution of the cluster shape as a function of the number of C atoms. A carbon hexamer (C_6) is a convenient system to illustrate our main findings. At this size, four motifs are basically in competition (illustrated in Figure 2a−e): a linear chain ($C_{6,L}$), a ring ($C_{6,R}$), a branched or starlike configuration ($C_{6,S}$) and a double-star configuration ($C_{6,DS}$). According to our DF approach, in the gas phase $C_{6,R}$ is the global minimum with an atomization energy of −35.02 eV, while $C_{6,L}$ is higher in energy by 0.23 eV and $C_{6,S}$ and $C_{6,DS}$ are not even local minima. The interaction with the surface drastically changes this energy ordering: $C_{6,L}$ is now much favored with an adsorption energy of E_{ads} = −42.0 eV, while $C_{6,R}$, $C_{6,S}$, and $C_{6,DS}$ are higher in energy by 1.32, 0.65, and 1.38 eV, respectively. This was found to be a general feature of small C clusters adsorbed on Ni(111): linear configurations are always favored with respect to ring or branched ones at least up to 10 C atoms;

Table 2. Diffusion Energy Barriers (E_{diff}, in eV) for Small Carbon Clusters (C_n, n = 1, 4) on the Ni(111) Surface Computed by the DF/NEB Method

process	E_{diff} (eV)
monomer hopping	0.38
dimer diffusion	0.58
linear trimer "in-channel" diffusion	0.46
linear trimer "cross-channel" diffusion	0.43
linear tetramer "in-channel" diffusion	0.20
linear tetramer "cross-channel" diffusion	0.35
"$C_{4,S}\{111\}_{fcc-fcc-fcc-top}$" tetramer diffusion	1.18
"$C_{4,S}\{111\}_{hcp-hcp-hcp-fcc}$" tetramer diffusion	0.76
$C_{4,S}$ dissociation into a trimer plus adatom	0.66

see Table 1 (12-atom and 14-atom clusters have also been investigated finding the same behavior, not reported in Table 1). In the gas phase, rings are generally favored over chains by a greater number of C−C bonds (they do not have unsaturated terminal atoms) and with few exceptions (size 8 and some odd sizes) are predicted to be the optimal morphology of gas-phase carbon clusters between 6 and 20−24 atoms (for larger clusters one finds a crossover to cagelike configurations).[23] In contrast, on the surface chains are favored with respect to rings because (i) terminal atoms are stabilized as they interact more strongly with the surface, (ii) rings are disfavored because they cannot adhere to the surface maintaining their optimal gas-phase configurations and simultaneously satisfying the constraints due to epitaxial relationships. Long enough rings can adopt a chain-like configuration resembling chains with four turning points, as shown for $C_{10,R}$ in Figure 2e, thereby decreasing the curvature energy so that the energy difference between chains and rings with more than 14 atoms will eventually tend to zero. However, long rings are not expected to play an important role in the growth process, as it is difficult to generate them from chains (which are formed initially as they are thermodynamically more stable and kinetically easier to produce) and are only marginally favored from a thermodynamic point of view with respect to chains for large aggregates. A similar reasoning applies to and discards the importance of double ring configurations, such as $C_{10,DR}$ in Figure 2f.

The key to nucleation of graphitic nanostructures will then be the conversion from chain to branched (or starlike) structures. On Ni(111), linear chains are oriented parallel to ⟨110⟩ surface directions. For example, dimers are best adsorbed on hcp−fcc hollow sites (see Figure 3a,c),[9] trimers on hcp−fcc−hcp sites (see Figure 3d), and analogous considerations hold for tetramers (see Figure 3e) and longer chains (see Figure 2b,d). Their stability is easily predicted as it is quickly converging as a function of chain length. The stability of branched arrangements is more difficult to predict. It should be stressed that in a starlike configuration the branching point is as a rule on-top a Ni atom (see a star−tetramer in Figure 3f), thus resembling one of the two C atoms in the top-fcc adsorption of a graphene monolayer. Also the C−C distances are nearly the same as in graphene. The starlike motif can thus be seen as a graphitic nucleus, which is not the case for chains. The difference with respect to graphene is that the three peripheral C atoms in the star are more of carbidic type, as confirmed by the fact that they are closer to the Ni surface, with a distance to the Ni plane of 1.18 Å, than the central carbon, with a distance of 1.65 Å—for comparison, the distance in graphene is

2.12 Å (this explains why van der Waals interactions are less crucial for the star configuration than for graphene). Energetically, star configurations are less stable than chain motifs for small clusters. However, as it will be suggested later on, their formation is a natural pathway from adatoms and chains to graphene.

Surface diffusion is known to be crucial for understanding epitaxial growth,[4] and we now turn attention to the kinetics of C aggregates on Ni(111), determining the elementary diffusion mechanisms and the corresponding energy barriers governing their mobility paths (pictorial views of diffusion mechanisms are provided in the Supporting Information). The calculated energy barriers (E_{diff}) for the diffusion of C clusters up to four atoms on the Ni(111) surface are given in Table 2. The barrier for single atom hops (0.38 eV) is in good agreement with the literature.[9,11] Since the lowest dimer energy configuration on the Ni(111) surfaces is on hcp−fcc hollow sites, dimers can diffuse by hopping from one ⟨110⟩ direction to another one, with the mechanism of the concerted mode shown in Figure 3a−c. The barrier is 0.58 eV, which is again in fair agreement with values from the literature.[5,9] The trimer almost equivalently migrates by sliding in a ⟨110⟩ direction or rotating toward a ⟨112⟩ direction with one atom on top, with energy barriers of 0.46 and 0.43 eV, respectively. The energy barrier for the tetramer chain is substantially lower (0.20 eV), with the sliding mechanism along ⟨110⟩ (barrier of 0.20 eV) favored over rotation toward a ⟨112⟩ direction (barrier of 0.35 eV). Other mechanisms involving, e.g., detachment of a terminal C atom from the linear tetramer and transformation in a trimer, diffusion of the fragments, and successive reformation of the tetramer (also associated with Ostwald ripening), have higher energy barriers, as tetramer dissociation already presents a barrier larger than 0.7 eV. Tetramer chains diffusing by sliding are thus much more mobile than either dimers or adatoms. This feature is not peculiar to the tetramer but is common to all longer chains. In contrast, the energy barrier for the diffusion of a star tetramer is rather high (1.18 eV), with the corresponding mechanism shown in Figure 3f−h. Again, the lower mobility of branched C aggregates is not peculiar to the tetramer. For example, a star hexamer (see Figure 2c) has a diffusion energy barrier of 1.14 eV with a diffusion mechanism essentially identical to that of the star tetramer (not shown). Mobility of branched C clusters via diffusion as a whole is in this case unfavorable with respect to cluster disruption: debinding of a central C atom from $C_{4,S}$ in fact has a barrier of 0.66 eV (see Table 2 and the Supporting Information), while the reverse process of adatom attachment to a trimer has a barrier of 0.40 eV.

The difference between diffusion mechanisms and energetics of linear and star configurations can be rationalized. A close look at panels b and g of Figure 2 and panels d and e of Figure 3 shows in fact that chains are not straight. The terminal atoms are closer to the surface plane (see Figure 3d′) and their distance to the surface is independent of the chain length. Hence, the weakening of the bonding to Ni is taken over by the other atoms and the migration energy of the terminal atoms is the limiting factor to diffusion. For this reason, the mobility of a chain with length over four atoms is little dependent on its length, and the final result is that long chains can diffuse much faster than adatoms. This is similar to what found for metal clusters diffusing on oxides,[24] with the clear distinction that in the latter case high mobility is basically associated with the lattice mismatch with respect to the substrate, whereas for carbon chains on Ni(111) high mobility is due to a change in the nature of the bonding with the metal (a chemical rather than a mechanical effect). Chains can thus slide along (110) and diffuse with barriers around 0.2−0.4 eV, whereas neither rings nor star configurations can perform this movement and are thus much less mobile (diffusion energy barriers around 1.0/1.5 eV).

Since the energy barriers for cross-channel hops are higher than those for in-channel sliding for chains longer than the tetramer, the diffusion of chains will be predominantly one-dimensional along ⟨110⟩ channels, and we can expect that during growth they will increase their length by collecting atoms along their path or by extracting atoms from subsurface sites. When a chain encounters an adatom in a nearest-neighbor channel, e.g., via adatom jump (see the trimer + adatom combination into $C_{4,S}$ in the Supporting Information), a curved (Figure 2c) or star (Figure 2d) configuration will result, the latter being more stable than the former. Similar starlike networks will arise when chains sliding along nearest-neighbor channels network by diffusion of terminal atoms over to the ridge of the channel.[10] Once formed, star configurations will diffuse more slowly and—especially at low temperature—will act as pinning centers and nucleation points for the formation of graphene-like structures. The kinetic stability of these configurations is further enhanced by the fact that energy barriers for transforming a starlike branching point into a chain are larger than those for star diffusion: for example the transformation energy barrier is 1.55 eV for a starlike into a curved linear hexamer according to our DF calculations (see the mechanism in Figure 2c,d). Once star or many-star configurations are formed it is thus difficult to get rid of them even if they are less stable than other arrangements. Moreover, for large aggregates graphene-like configurations (i.e., many-star arrangements) will eventually overcome chainlike ones also from a thermodynamic point of view due the greater stability of their C−C bonding. The key role assigned to chains (and to their interplay with carbon networks) in the initial stages of growth in the present picture is in tune with growth models based on empirical Hamiltonians in which chains were found to be a common occurrence, even though the mobility of branched configurations was predicted to be different from our findings.[20]

CONCLUSIONS

We investigate via first-principles simulations the low-energy configurations of C aggregates up to 10 atoms on Ni(111), which can be building blocks in the growth of graphene, finding a thermodynamic preference for chain configurations. Their mobility on the regular (undefected) Ni(111) surface is examined in order to understand the kinetic paths leading to nuclei formation, finding that carbon chains can diffuse faster than single adatoms. A model of nucleation of growth is then proposed in which incoming C atoms generate chains which diffuse rapidly along (110) directions and grow by successive encounters with less mobile adatoms in their channel until they meet in an unfavorable configuration to grow as chains and start networking giving rise to starlike branching points. The star motif presents one atom in the characteristic on-top adsorption and is the prodrome of graphene. Star configurations are much less mobile and are kinetically robust (presenting higher energy barriers for interconversion into other species) and thus act as the nuclei of growth. The key role assigned to diffusion in this model is in agreement with the experimentally determined apparent activation energies.[3] It is expected that in proper experimental conditions, depending on the size of the terraces on the Ni surface, the

density of surface defects and the growth parameters, in particular the temperature and the input rate of carbon species (incoming flux from external deposition or from internal storage sites—whichever subsurface or defects), the proposed homogeneous nucleation mechanism can be competitive with the usually assumed one based on heterogeneous nucleation. Indeed it has very recently been shown[8] that large-area single crystal monolayer graphene, of great interest in applications, can be obtained on Ni(111) one-monolayer-thick flat terraces. The proposed mechanism, apart from shedding new light on the thermodynamic and kinetic processes behind the growth of carbon nanomaterials, should also be particularly relevant at low temperature and/or in plasma-enhanced chemical vapor deposition, thus in conditions which are currently targeted as more economical and beneficial to enable use of more sensitive substrates and/or to better control the growth kinetics.[3]

METHODS

Our computational approach is based on density-functional (DF) spin-unrestricted calculations using a plane wave basis set,[25] a gradient-corrected exchange-correlation functional (the Perdew−Burke−Ernzerhof one, PBE)[26] and ultrasoft pseudopotentials.[27] An energy cutoff of 40 Ry is used for selection of the plane wave basis set for describing the wave function (and 400 Ry for describing the electron density) and a mesh of 2 × 2 × 1 k-points. Extensive calculations with larger cutoffs and k-meshes showed that convergence with respect to these numerical parameters is achieved within 0.05 eV, as also confirmed by the excellent agreement of the present results with previous calculations (see the section on Comparison with Previous Work). For example, the adsorption energy of a single C atom on a hcp site of Ni(111) is −6.71 eV using an energy cutoff of 60 Ry and a 4 × 4 × 1 k-mesh. The size of the Ni(111) supercell is at least 3 × 3 for a single C atom adsorption and up to 9 × 3 for the longer C chains to ensure that distances between carbon atoms in neighboring cells are larger than 7−8 Å, so that their interaction can be altogether neglected. van der Waals (dispersion) contributions are systematically tested using an empirical correction[15] to the PBE total energy and forces, but found to be crucial only for the adhesion of a graphene monolayer in which the contributions due to direct chemical bond become very small. A dipole correction[28] was also applied in many test calculations to cancel spurious intercell polarization effects but found to give negligible contributions. A slab of five Ni layers is used to describe the Ni surfaces with the bottom three layers kept frozen at their bulk position (experimental lattice parameter of 2.49 Å, practically identical to the DF-predicted one). Selected calculations with a larger number of layers (up to eight) gave essentially the same results in the case of surface adsorption, whereas in the case of subsurface adsorption they exhibited differences slowly converging with the number of layers due to the elastic contributions discussed in the Results and Discussion section.

The climbing image nudged elastic band method[29] is used to determine the energy barriers of diffusion processes. This method searches for the minimum energy path between two local minima by creating a fixed number of intermediate configurations (images) that are linked to each other by elastic springs. The image highest in energy does not feel the spring forces along the band; instead, the true force at this image along the tangent is inverted. In this way, the image tries to maximize its energy along the band, and thus when this image converges it is at the exact saddle point. The local minima singled out by total energy search are set as starting configurations of the NEB procedure using seven intermediate images, which is sufficient to produce very accurate results.[29]

As discussed in the Results and Discussion section, it is important to quantitatively assess the competition between surface and subsurface adsorption. For a C dimer, subsurface adsorption leads to a repulsion by 1 eV with respect to isolated subsurface C atoms according to our DF approach. The small size of the unit cell could bias this result by overestimating the strain component in the Ni lattice for subsurface with respect to epitaxial adsorption. To estimate the relaxation in elastic stress due to the cell size, we calculated the difference in elastic energy stored in the Ni lattice between subsurface adsorption of a C dimer in a (3 × 3) unit cell with 5 Ni layers and a large (9 × 9) unit cell with 18 layers via classical force-fields. A Morse function fitted on the DF-calculated energy curve was used for the C−C binding in the C_2 dimer, a tight-binding second-moment-approximation empirical potential for Ni−Ni bonding,[30] and a purposely derived force field based on a Morse analytic form and fitted on DF simulations for the C−Ni interaction (details are available upon request). The difference in elastic energy came out to be 0.5 eV, as discussed in the main text, thus unable to revert the greater stability of an ad-dimer with respect to a subsurface dimer.

ASSOCIATED CONTENT

Supporting Information. The detailed structure of selected C clusters and their diffusion mechanisms on the Ni(111) surface. This material is available free of charge via the Internet at http://pubs.acs.org.

AUTHOR INFORMATION

Corresponding Author
*E-mail: alessandro.fortunelli@cnr.it.

ACKNOWLEDGMENT

This work has been performed in part under the HPC-EUROPA2 project (project number: 228398) with the support of the European Commission—Capacities Area—Research Infrastructures. A.F. acknowledges financial support from the ERC-AG SEPON project and computational support at CINECA supercomputing center within an agreement with Italian CNR. Partial support is also acknowledged from the FRS-FNRS of Belgium under agreement ref 2.4514.08.D.C. gratefully acknowledges support from the Foundation of Excellent Doctoral Dissertation of Beijing City (No. YB20091001001).

REFERENCES

(1) Baughman, R. H.; Zakhidov, A. A.; de Heer, W. A. *Science* **2002**, *297*, 787.
(2) Castro Neto, A. H.; Guinea, F.; Peres, N. M. R.; Novoselov, K. S.; Geim, A. K. *Rev. Mod. Phys.* **2009**, *81*, 109.
(3) Hofmann, S.; Csányi, G.; Ferrari, A. C.; Payne, M. C.; Robertson, J. *Phys. Rev. Lett.* **2005**, *95*, 036101.
(4) Michely, T.; Krug, J. *Islands, Mounds and Atoms*; Springer: Berlin, 2004.
(5) Abild Pedersen, F.; Norskov, J. K.; Rostrup Nielsen, J. R.; Sehested, J.; Helveg, S. *Phys. Rev. B* **2006**, *73*, 1154191.

(6) Moors, M.; Amara, H.; de Bocarme, T. V.; Bichara, C.; Ducastelle, F.; Kruse, N.; Charlier, J. C. *ACS Nano* **2009**, *3*, 511.
(7) Cheng, D.; Hou, M.; Moors, M.; de Bocarme, T. V.; Kruse, N. *Chem. Phys. Lett.* **2010**, *492*, 63.
(8) Iwasaki, T.; Park, H. J.; Konuma, M.; Lee, D. S.; Smet, J. H.; Starke, U. *Nano Lett.* **2011**, *11*, 79.
(9) Yazyev, O. V.; Pasquarello, A. *Phys. Rev. Lett.* **2008**, *100*, 156102.
(10) Wang, S. G.; Liao, X. Y.; Cao, D. B.; Li, Y. W.; Wang, J.; Jiao, H. *J. Phys. Chem. C* **2007**, *111*, 10894.
(11) Shin, Y. H.; Hong, S. *Appl. Phys. Lett.* **2008**, *92*, 043103.
(12) Zhang, Q. M.; Wells, J. C.; Gong, X. G.; Zhang, Z. *Phys. Rev. B* **2004**, *69*, 205413.
(13) Cinquini, F.; Delbecq, F.; Sautet, P. *Phys. Chem. Chem. Phys.* **2009**, *11*, 11546.
(14) Wiltner, A.; Linsmeier, C.; Jacob, T. *J. Chem. Phys.* **2008**, *129*, 084704.
(15) Barone, V.; Casarin, M.; Forrer, D.; Pavone, M.; Sambi, M.; Cittadini, A. *J. Comput. Chem.* **2008**, *30*, 934.
(16) Gamo, Y.; Nagashima, A.; Wakabayashi, N.; Terai, M.; Oshima, C. *Surf. Sci.* **1997**, *374*, 61.
(17) Fuentes-Cabrera, M.; Baskes, M. I.; Melechko, A. V.; Simpson, M. L. *Phys. Rev. B* **2008**, *77*, 035405.
(18) Papagno, L.; Conti, M.; Caputi, L. S.; Anderson, J.; Lapeyre, G. J. *Phys. Rev. B* **1991**, *44*, 1904.
(19) Lin, M.; Tan, J. P. Y.; Boothroyd, C.; Loh, K. P.; Tok, E. S.; Foo, Y. L. *Nano Lett.* **2006**, *6*, 449.
(20) Amara, H.; Bichara, C.; Ducastelle, F. *Phys. Rev. Lett.* **2008**, *100*, 056105.
(21) Deck, C. P.; Vecchio, K. *Carbon* **2006**, *44*, 267.
(22) Brjesson, A.; Zhu, W.; Amara, H.; Bichara, C.; Bolton, K. *Nano Lett.* **2009**, *9*, 1117.
(23) Jones, R. O.; Seifert, G. *Phys. Rev. Lett.* **1997**, *79*, 443.
(24) Barcaro, G.; Fortunelli, A.; Nita, F.; Ferrando, R. *Phys. Rev. Lett.* **2005**, *95*, 246103.
(25) Giannozzi, P.; Baroni, S.; Bonini, N.; Calandra, M.; Car, R.; Cavazzoni, C.; Ceresoli, D.; Chiarotti, G.; Cococcioni, M.; Dabo, I.; Dal Corso, A.; de Gironcoli, S.; Fabris, S.; Fratesi, G.; Gebauer, R.; Gerstmann, U.; Gougoussis, C.; Kokalj, A.; Lazzeri, M.; Martin Samos, L.; Marzari, N.; Mauri, F.; Mazzarello, R.; Paolini, S.; Pasquarello, A.; Paulatto, L.; Sbraccia, C.; Scandolo, S.; Sclauzero, G.; Seitsonen, A. P.; Smogunov, A.; Umari, P.; Wentzcovitch, R. M. *J. Phys.: Condens. Matter* **2009**, *21*, 395502.
(26) Perdew, J. P.; Burke, K.; Ernzerhof, M. *Phys. Rev. Lett.* **1996**, *77*, 3865.
(27) Vanderbilt, D. *Phys. Rev. B* **1990**, *41*, 7892.
(28) Bengtsson, L. *Phys. Rev. B* **1999**, *59*, 12301.
(29) Henkelman, G.; Uberuaga, B. P.; Jónsson, H. *J. Chem. Phys.* **2000**, *113*, 9901.
(30) Cleri, F.; Rosato, V. *Phys. Rev. B* **1993**, *48*, 22.